Deform to Inform: Persistent Batteryless Sensing via Antenna Deformation and RFID Impedance Adaptation

Haochen Zhao
University of California, Los Angeles
zhaohch@ucla.edu

Vishnu Naidu
University of California, San Diego
vrnaidu@ucsd.edu

Shanmu Wang
University of California, Los Angeles
shanmu@cs.ucla.edu

Kenneth J. Loh
University of California, San Diego
kjloh@ucsd.edu

Omid Abari
University of California, Los Angeles
omid@cs.ucla.edu

Abstract

A stable environment is critical for preserving product quality in industries such as pharmaceuticals and perishable goods logistics. While current RFID-based sensors enable wireless monitoring of temperature and moisture, they lack the ability to record threshold violations without continuous reader power or battery-supported logging. This paper presents AntSense, a battery-free RFID sensor that leverages stimuli-responsive structures to physically record environment violation events during the transit even when there is no reader available. When exposed to temperature or moisture beyond thresholds, memory alloy or solvable materials undergo irreversible geometric deformation, altering the integrated antenna's characteristics. These changes remain detectable via standard RFID readers even after environment conditions normalize, enabling verification of transit integrity. Our prototype evaluations demonstrate reliable detection of threshold violations in real-world scenarios. By combining passive operation with persistent event recording, AntSense offers a scalable solution for supply chain monitoring without compromising the maintenance-free advantages of RFID technology.

CCS Concepts

• **Hardware → Sensors and actuators**; **Wireless integrated network sensors**.

Keywords

RFID, Environment Monitor, Wireless Sensor

ACM Reference Format:
Haochen Zhao, Vishnu Naidu, Shanmu Wang, Kenneth J. Loh, and Omid Abari. 2026. Deform to Inform: Persistent Batteryless Sensing via Antenna Deformation and RFID Impedance Adaptation. In . ACM, New York, NY, USA, 14 pages. https://doi.org/10.1145/nnnnnnn.nnnnnnn

Conference'17, July 2017, Washington, DC, USA

ACM ISBN 978-x-xxxx-xxxx-x/YY/MM
https://doi.org/10.1145/nnnnnnn.nnnnnnn

1 Introduction

Monitoring environmental conditions such as temperature and moisture is critical, as even brief exposure to unfavorable conditions can degrade product quality or safety [1, 21, 22, 25, 42]. In many applications, detecting whether a threshold violation occurred is essential [11, 36, 56]. For example, perishable foods must not be exposed to freezing temperatures or contaminants, and pharmaceuticals can become ineffective or harmful after a single excursion beyond prescribed temperature or humidity limits [36]. While the logistics industry invests heavily in infrastructure and procedures to maintain stable conditions during the transit [14, 27], internal environments often remain not guaranteed, requiring collaboration between multiple parties for data handling and continuous monitoring [10, 46, 54]. Therefore, a self-contained solution that can verify whether a shipment remained within safe limits (i.e., no deviation from permitted temperature or dryness) throughout transit is essential and highly desirable. While active solutions powered by batteries are available, a passive solution without any battery is very valuable since batteries are not environmentally sustainable and raise safety concerns.

Traditional passive solutions rely on visual indicators that change color or properties upon exposure to environmental stimuli [8]. However, these require line-of-sight inspection, limiting scalability and throughput in large logistics operations. Wireless solutions, particularly **R**adio **F**requency **ID**entification (RFID) based, offer significant advantages for supply chain monitoring [17, 24, 37]. For example, passive RFID-based sensing has been explored for detecting temperature, moisture, displacement, and material changes [12, 15, 26, 34, 41, 43, 45, 52, 53]. However, these techniques only provide *instantaneous* measurements. Once the power is removed (i.e., no reader is close by), measurements are not possible, making it impossible to determine whether a threshold violation occurred during transit.

One approach to solve this is to deploy RFID readers inside every transport vehicle, but this is costly and impractical. Another option is to use battery-powered active radios or integrate a battery into each RFID tag, allowing it to monitor continuously and log events internally. However, this compromises the passive nature of the system and introduces high initial and maintenance costs. We aim to answer the question: *How to develop a scalable, low-cost, passive approach to detect the threshold violation event during the transit?*

This paper presents AntSense, a persistent batteryless sensor using RFID and stimuli-responsive materials. Stimuli-responsive materials undergo permanent or semi-permanent deformation when

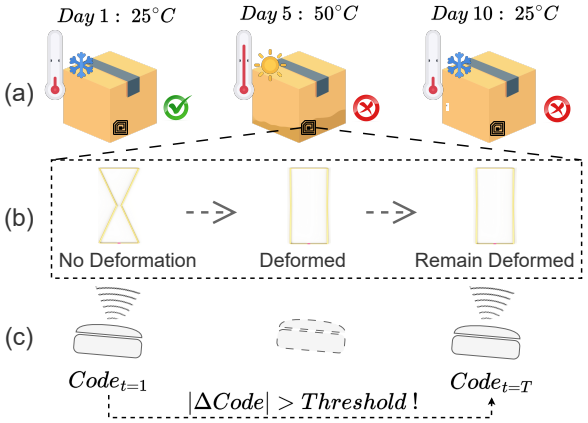

Figure 1: AntSense Threshold-Violation Event Detection. The figure shows the end-to-end system for AntSense. (a) An example application where a shipping box (containing food or medicine) is exposed to moisture/high temperature on Day 5 but later dries/cools down. (b) The instantaneous deformation of AntSense tag's antenna caused by moisture/high temperature, preserving a record of the threshold-violation event. (c) An RFID reader detects and decodes the tag's deformation, retrieving the stored information about past environmental conditions.

exposed to environmental triggers such as temperature or moisture. Hence, by integrating an antenna and an RFID chip into these materials, their deformations can be detected wirelessly with a commercial RFID reader. Specifically, the deformation impacts the impedance of the antenna, which causes the RFID chip to automatically adjust its impedance to maximize power transfer efficiency. This change is stored in an RFID tag's register, which can be read by commercial RFID readers. Unlike traditional RFID-based sensors, AntSense retains records of threshold violations without requiring batteries or continuous reader presence. Finally, it worth mentioning that although some past work has integrated stimuli-responsive materiel into the antenna design of an RFID tag, they either do not provide persistent sensing without power (i.e. their antenna does not deform, and hence lack passive memory) [32, 39, 43], or/and they do not work seamlessly with commercial RFID readers and EPC protocol [5, 13, 18, 31]. In contrast, we introduce the first single-chip persistent batteryless sensor that uses the impedance matching code accessible in commercial RFID readers and chips. Our sensor is capable of detecting if a temperature has exceeded a threshold or if the sensor has been exposed to moisture.

We design and prototype an end-to-end prototype of AntSense, using *shape memory alloy* and *solvable material* and commercial RFID chips and reader. Experimental results demonstrate that AntSense is able to successfully record and report different predefined temperature threshold and moisture violations, while maintaining high robustness across varying reading angles, distances, mobility, and surrounding materials.

To summarize, this paper makes the following contributions:

- We introduce AntSense, a persistent passive RFID sensor that uses stimuli-responsive materials to physically record environmental changes even when there is no reader available.
- We design and fabricate structures using stimuli-responsive materials and integrate a single standard EPC RFID chip and antenna into the structure.
- We propose a new mechanism to enable RFID reader to sense the tag's antenna deformation, and compare our approach with RSS-based, phase-based sensing through both simulation and real-world measurements.
- We evaluated the performance of AntSense empirically in detecting temperature changes and moisture contact . We also show its robustness in dynamic environments and various other adverse scenarios.

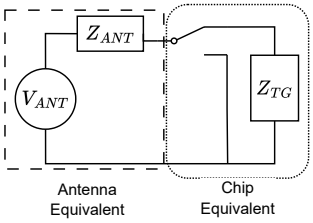

Figure 2: Tag chip receiving equivalent circuit

2 Background

2.1 RFID Overview

A UHF RFID system operates as a passive backscattering system. It consists of an active participant, the reader, and one or multiple passive participants, the tags. Backscatter communication transmits data from the tags to the reader. The tag selectively reflects the continuous carrier wave transmitted by the reader. The two different states of reflected signal represent data bits. This design simplifies the tag hardware, requiring only an RF switch for modulation, allowing the tag to remain fully passive and operate without external power sources.

To adapt RFID for sensing applications, it is essential to understand the entire communication chain. We follow the energy flow from the reader to the tag and back to the reader to model the process comprehensively. In this model, abbreviations are used as follows: RD for reader, TG for tag, RX for receiving, and TX for transmitting. Symbols used include P for *power*, G for antenna *gain*, and h for complex channel response.

The wireless transmission over the air is modeled as follows:

$$\begin{aligned} P_{RX}^{TG} &= P_{TX}^{RD} \cdot G^{RD} \cdot |h|^2 \cdot G^{TG} \\ P_{RX}^{RD} &= P_{TX}^{TG} \cdot G^{TG} \cdot |h|^2 \cdot G^{RD} \end{aligned} \tag{1}$$

where P_{TX}^{RD} and P_{TX}^{TG} represent the transmitted power from the reader and tag, G^{RD} and G^{TG} denote the antenna gains of the reader and tag. The amplitude of complex channel response h depicts the energy loss in air channel. The power received at the tag powers the tag circuitry and carries backscatter transmission, while the signal received back at the reader is used to decode the tag's data.

2.2 RFID Tag Equivalent Circuit

Here we take a close look at the tag, where sensing will take place. The tag's chip load is complex, denoted as $Z^{TG} = R^{TG} + jX^{TG}$. Similarly, the antenna has a complex radiation impedance $Z^{ANT} = R^{ANT} + jX^{ANT}$. During energy harvesting, when energy flows from the antenna to the chip, the power absorbed (higher is better) by the chip is given by [38]:

$$P^{TG}_{chip} = P^{TG}_{RX} \cdot (1 - |\Gamma^{chip}|^2) \tag{2}$$

where Γ^{chip} is the complex power reflection coefficient (lower amplitude is better) between the chip and the antenna [47], defined as:

$$\Gamma^{chip} = \frac{Z^{TG} - \overline{Z^{ANT}}}{Z^{TG} + Z^{ANT}} \tag{3}$$

From Equation 2, we observe that the power absorbed by the chip is maximized when the reflection coefficient is zero. According to Equation 3, this occurs when $Z^{TG} = \overline{Z^{ANT}}$, meaning the chip impedance is the complex conjugate of the antenna impedance. This principle, known as impedance matching, is a key consideration in any tag design.

The phase of the radio wave follows a similar structure to Equation 1. In free space, it mirrors the same equations, with power terms replaced by phase angles and products replaced by summations. Within the tag, the phase delay corresponds to the angle of the reflection coefficient Γ^{chip}.

By playing with all these parameters, we can propose many different schemes to detect the change remotely. They will be examined in the feature selection section.

3 AntSense Overview

We present AntSense, a novel battery-free sensing system that retains the record of threshold-violation events. Figure 3 illustrates our sensing scheme.

The core idea behind AntSense is to leverage stimulus-responsive materials that undergo permanent deformation when exposed to environmental stimulus. Here permanent deformation means that it will remain at the same shape even when the temperature or moisture level returns to normal. Therefore, this deformation effectively records the occurrence of an event in the past.

To enable large-scale, wireless detection, we integrate these materials with an RFID chip and antenna. Our design follows two approaches in parallel: the temperature one uses the stimulus-responsive material as the antenna itself and the moisture one embeds an antenna within a deformable structure. When the material deforms, it alters key antenna properties. An RFID chip connected to the antenna captures these changes, allowing a standard RFID reader to wirelessly detect variations in the antenna. By analyzing these responses, we can infer whether a threshold violation occurred, providing a simple and scalable sensing solution for monitoring conditions during transit.

The rest of the paper details our design methodology. In Section 4, we describe the selection and fabrication of stimulus-responsive structures. Section 5 explains how the antenna is integrated into the system. Section 6 covers the connection between the antenna and the RFID chip to enable wireless sensing. Finally, we evaluate the system's performance in Section 7.

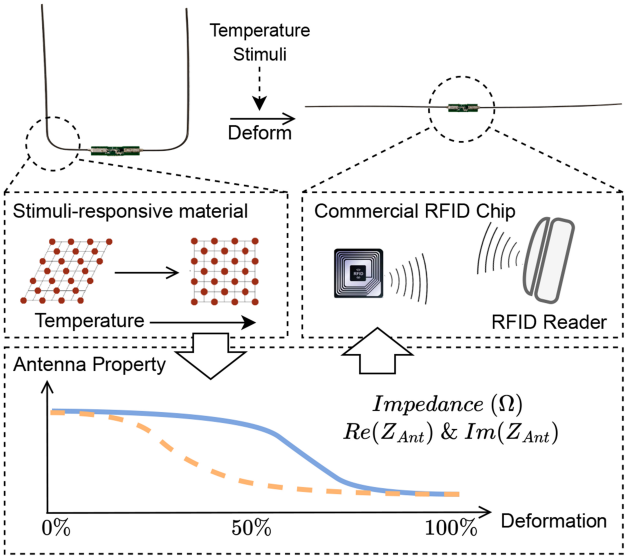

Figure 3: AntSense's Sensing Scheme. The principle of AntSense is to integrate stimulus-responsive materials with an RF antenna, either by using the material as the antenna itself or embedding an antenna within a deformable structure. When exposed to environmental stimuli, the material deforms, altering the antenna's properties. These changes can be detected through RFID responses, enabling large-scale, wireless measurement of deformation.

4 Stimuli-Responsive Structure Design

In this paper, we focus on detecting temperature and moisture violations, two of the most common environmental risks in the shipping industry [1]. To achieve this, the tag structures meet two key requirements: (a) They must change shape in response to temperature or moisture, effectively recording whether a violation has occurred. (b) They must accommodate antenna and RFID chip integration, allowing an RFID reader to wirelessly detect these changes.

To meet these requirements, we leverage two types of stimuli-responsive materials: *shape memory alloys (SMAs)* for temperature sensing and *water-soluble materials* for moisture sensing. By carefully designing these materials into special structures, we ensure both reliable stimulus response and seamless antenna integration.

4.1 Temperature

Shape Deformation in Response to Temperature: Among various stimuli-responsive materials, *Shape Memory Alloys (SMAs)* are particularly well-suited for temperature sensing due to their low cost (1 dollar per foot for retail), high sensitivity, and ability to retain deformations. SMAs exhibit a thermal shape memory effect, meaning they can switch between two stable solid phases depending on temperature. Specifically:

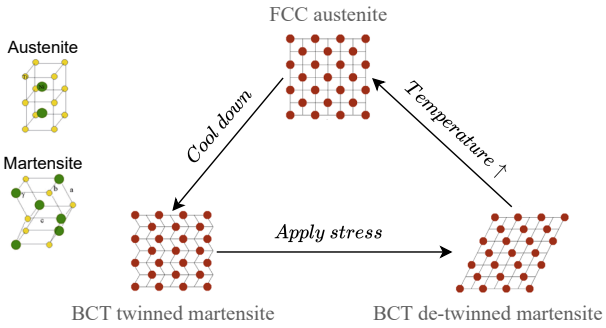

Figure 4: The State Transition of SMA Materials. When temperature is low, SMA exists in the BCT martensite phase, and can be reshaped through stress. When the temperature is higher than the transformation threshold, the SMA transits to the FCC austenite phase and remain in that shape even after cooling down.

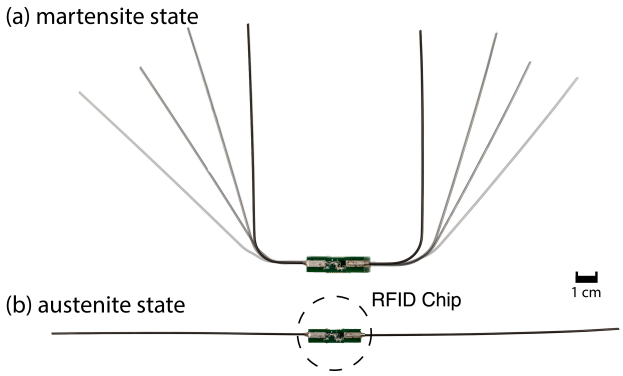

Figure 5: The Deformation of the Temperature Tag. The deformed tag (austenite state) is 0.5×24.5 cm^2 and 1.24 g

- At low temperatures, SMAs exist in the *martensite phase*, where the material has a body-centered tetragonal (BCT) crystal structure. In this phase, the material is highly deformable, allowing it to be reshaped through stress. This reshape is called de-twinning.
- At high temperatures, SMAs transition to the *austenite phase*, characterized by a face-centered cubic (FCC) crystal structure. When heated above the transformation temperature, the material returns to its preset austenite shape and remains in that shape even after cooling below the transformation temperature.

Figure 4 exemplifies these transitions. This transformation allows SMA-based structures to function as event recorders. If the material has deformed into its austenite shape, it indicates that the temperature threshold was exceeded. By selecting an appropriate transformation temperature, we can determine whether a temperature violation occurred during transit.

Integration with an Antenna: SMA nickel titanium (nitinol) wire possesses electrical properties that are comparable to a copper antenna, which makes it possible to function as the dipole antenna itself. Specifically, we choose nitinol straight wire with a diameter of

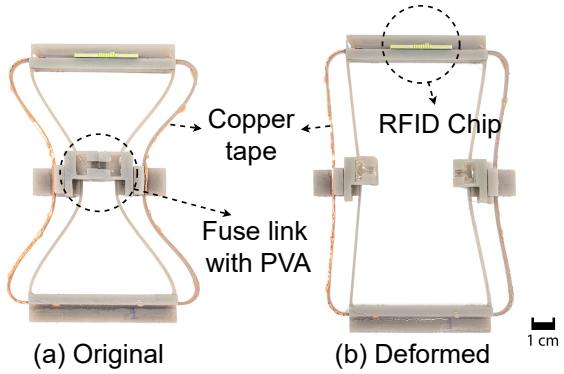

Figure 6: The Deformation of the Moisture Tag. The deformed moisture tag is 7.8×11.3 cm^2 and 14.50 g

∅1.0 mm, as it is still lightweight and provides enough mechanical strength.

To create a temperature-sensitive tag, we use an SMA wire which is a straight wire in the austenite phase (FCC structure), and bend it into a deformed shape while in its low-temperature martensite phase (BCT structure), as shown in Figure 5(a).

When exposed to temperatures above the transformation threshold, the SMA wire returns to its original straight shape in the austenite phase (FCC structure), as shown in Figure 5(b), which is now functioning as a common dipole antenna. Since the wire itself functions as the antenna, its deformation naturally alters its electromagnetic properties, which can be detected wirelessly through RFID interrogation.

Current commercially available SMA covers a trigger temperature ranging from -30 °C to 80 °C. In our application scenario, we experiment with transformation temperatures of 40°C, 50°C, and 80°C. Different critical temperatures can be achieved by selecting alternative SMA compositions, making this approach adaptable for applications for frozen and refrigerated goods storage. We choose this SMA implementation for its simplicity, low-cost and its potential of using partial deformation to record temperature in finer granularity.

4.2 Moisture

Shape Deformation in Response to Moisture: Unlike temperature-sensitive materials, no existing material directly changes shape upon water exposure while maintaining both sufficient mechanical strength and suitable antenna properties. To address this, we design a *compliant mechanism* combined with *water-soluble materials*, allowing structural deformation after moisture exposure while ensuring compatibility with antenna integration. Our design consists of four compliant beams, a fuse link, and two fuse link holders, as shown in Figure 6. The fuse link, made of a water-soluble material, is secured by the two fuse link holders and maintains tension in the closed position. When exposed to moisture, the fuse link dissolves, releasing tension and triggering structural deformation.

Material Selection and Fabrication: For reliable moisture sensing, the fuse link must dissolve predictably upon exposure to water while maintaining mechanical integrity in dry conditions.

We use *polyvinyl alcohol (PVA)* due to its *water solubility, tunable dissolution rate*, and *strong mechanical properties*. PVA's hydroxyl (-OH) groups enable strong hydrogen bonding with water, accelerating dissolution upon exposure. One key factor in PVA's performance is its concentration, which affects both strength and solubility. Higher concentrations increase durability but slow down dissolution. Lower concentrations dissolve quickly but may be too fragile for prolonged operation. We use a concentration of 0.5M that provides an optimal balance of strength and dissolution rate, making it the preferred choice for our application.

We fabricate the compliant mechanism and fuse link holders using 3D-printed FormLabs Tough 1500 resin, which provides both durability and flexibility. To create the fuse link, PVA is dissolved in deionized water at 80–90°C while stirring continuously for 30–60 minutes to ensure uniformity. The solution is then cast into thin films within the fuse link holders and allowed to dry. We evaluate these films based on dissolution rate and tensile strength, ensuring stability under dry conditions while allowing controlled degradation when exposed to water.

Our current design aim at sensitivity to moisture in liquid form. This is done by using water soluble PVA for fuse links. However, it can be extended to sensing humidity in the surrounding air via different material selection that lose mechanical strength with exposed to water vapor in the air like polymers.

Integration with an Antenna: Our design enables seamless RF antenna integration. We add an antenna substrate to the tag, where a 3.8mm-wide copper tape with adhesive backing is attached to form a loop antenna. In normal conditions (Figure 6(a)), the PVA fuse link holds the structure in a closed state, maintaining the antenna's original shape and properties. When exposed to water, the fuse link dissolves, breaking the structural tension and allowing the compliant mechanism to open (Figure 6(b)). This deformation alters the loop antenna's geometry, changing its electromagnetic properties. The RFID reader detects this change through RFID's response, providing a wireless and scalable method for detecting moisture exposure.

5 Antenna Deformation as a Sensor

The deformation of the material records the stimuli from the environment. To enable remote and large-scale reading, we couple the deformation to the antenna properties, and integrate an RFID chip to reveal the antenna properties wirelessly. In this section, we focus on coupling the deformation to the antenna properties. Specifically, we first simulate how the antenna properties are affected after deformation, and then elaborate the antenna design principle for our sensing applications.

5.1 Simulation Setup

We start with the simulation on how the deformation would change the properties of two common types of antennas: a dipole (Figure 8a) and a loop (Figure 8b). We use Ansys HFSS to simulate the how the antenna properties changes with deformation. The frequency was set to 915Mhz, center of the RFID band in the United States. We conduct the simulation where the dipole antenna is bent from a common dipole antenna to a fully bent one when the two sides are on top of each other. Similarly, the loop antenna is bent from a rectangle $40 \times 140\ \text{mm}^2$ loop to a Σ shape, with the two long edges bent inward. We place a chip in the center of the dipole and in the center of one 40 mm edge of the loop antenna, respectively, assuming a chip load of $2073\Omega \parallel 2.4\,\text{pF}$. During the deformation, we record the antenna peak gains, complex impedance, and the reflection coefficients.

5.2 Gain and Impedance Responses to Deformation

Gain and impedance are critical parameters defining antenna performance, as shown in Equation 1 and Equation 3. Our simulations reveal:

For dipole antennas (Figure 7a, Figure 7b):

- Impedance: Both real and imaginary parts decrease with deformation
- Efficiency: Decrease monotonically due to mismatched chip impedance
- Gain: Remain constant until almost full deformation, then decreased

For loop antennas (Figure 7c, Figure 7d):

- Impedance: Real part decrease while and imaginary part increase when deviating from a rectangle loop
- Efficiency: Decrease as the loop bent
- Gain: Remain stable throughout deformation

These results suggest that maintaining good communication performance during sensing requires dynamic adjustment of chip impedance. Change in gain can be used easily by observing received signal strength indicator (RSSI). Changes in impedance can be leveraged as a sensing mechanism, particularly for dipole antennas before extreme deformation occurs.

The readout mechanism will be designed corresponding to the antenna property of interest. A gain change can be read by RSSI or minimal response power to read the tag. An impedance change can be read by observing RSSI and phase over frequency, or read back the chip internal turning capacitor value.

6 Detecting Antenna Deformation using RFID

Thus far, we have described how our sensor structure deforms in response to environmental stimuli and how this deformation can alter an antenna's properties. In this section, we explain how we integrate an RFID chip into the system to remotely measure these changes and infer deformation events.

6.1 Feature selection

To ensure compatibility with existing RFID infrastructure, we analyze the features provided by commercial RFID systems and identify the most suitable ones for sensing deformation. The key features available include:

- **Received Signal Strength Indicator (RSSI)** Measures signal power received from the tag, influenced by both channel conditions and tag deformation.
- **Phase** Captures effective length changes in the transmission path but is sensitive to multipath effects.
- **Matching Capacitance** Available in modern RFID chips, this feature allows the chip to adaptively tune its impedance

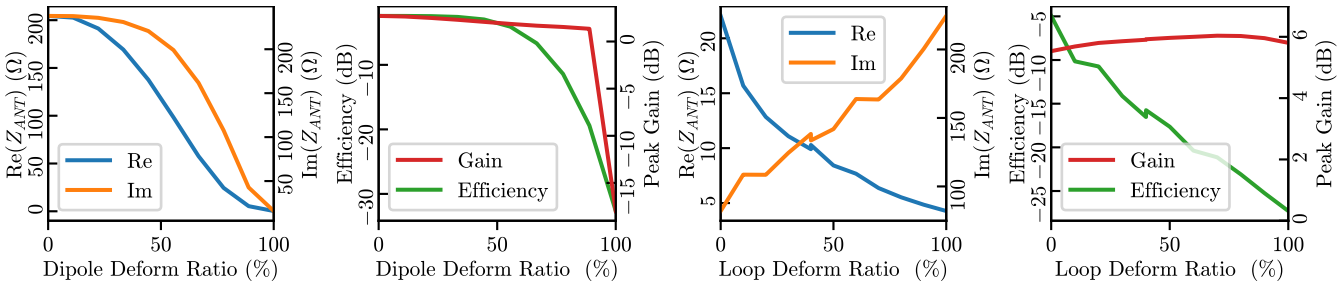

(a) Dipole Impedance **(b) Dipole Gain and efficiency** **(c) Loop Impedance** **(d) Loop Gain and efficiency**

Figure 7: Antenna Impedance, Gain, and Calculated Efficiency for Given Chip Impedance at Different Deformation Levels for Dipole (a)(b) and Loop (c)(d). Gain remained stable until much deformation, significant impedence and efficiency changes happened after deformation.

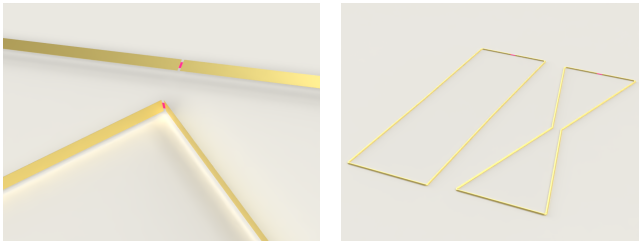

(a) Non deformed dipole (up), half deformed dipole (down)

(b) Non deformed Loop (right), fully deformed (left)

Figure 8: Visualization of undeformed and deformed (a) dipole and (b) loop antenna studied in the simulation

to optimize power transfer, revealing changes in antenna properties.

For RSSI and phase, they are widely available for RFID readers and we captured them with an Impinj R420 reader [19]. For matching capacitance, we use Magnus-S3 RFID chips [3], which provide 512 tuning levels (9-bit resolution) for matching capacitance adjustments. The 9-bit value is named *sensor code*. By monitoring this value, we can infer the level of deformation. Additionally, the chips offer an internal power indicator, which helps dynamically adjust reading power, preventing excessive amount of available energy causing the chip to de-tune itself as a protection.

To assess the sensitivity and stability of these features, we conducted preliminary experiments, evaluating how deformation affects each parameter and how robust they remain under varying conditions. Sensitivity was evaluated by folding commercial off-the-shelf tags with dipole antennas (onsemi SPS1T001PET) to various levels. For stability, we evaluated the tag at different distances and receiving power levels and with objects moving in vicinity.

Sensitivity: Figure 9 concludes the preliminary experiments on how deformation affects every of the three available RFID features. Figure 9a shows RSSI decreased steadily with more deformation, with a total 7.5 dB loss from minimal to maximum deformation tested. This 7.5 dB loss is equivalent to the loss caused by a 50% increase in distance, which will affect the readable range considerably. Figure 9b shows phase changed non-monotonically with deformation, making it hard to interpret data unambiguously. Figure 9c shows matching capacitance dropped with more deformation, with more sensitivity in the high-deformation region.

Both RSSI and sensing code make good candidates as they change significantly and monotonically in response to deformation. We continue to test their robustness against different cases of mobility.

Stability: We evaluated distance and mobility stability by varying the tag-reader distance and by moving a human tester near the stationary reader and tag. The results are shown in Figure 10, where the left column shows influence of moving object and right column showing influence of moving tag distances.

As distance increases, RSSI drops as the channel experiences more path loss. Phase suffered significant variations due to the extra phase delay. The sensing code changes only significantly at close distance, and stays almost constant at farther distance. At close distance, too much power is available to the chip, which might damage the chip. The change in sensor code can be explained as it slightly de-tunes itself to prevent damages. Therefore, to allow reliable reading in close range, lowering the transmission power is necessary.

Variations with environment with moving objects are significant for RSSI (Figure 10a) and phase (Figure 10c). With a standard deviation of 0.87 dB for RSSI and 11.12 degrees for phase, the two features show slightly deteriorated performance when operating in environment with mobility. The sensor code distribution is shown in Figure 10e , with a standard deviation of 2.94.

The susceptibilities of RSSI and phase are explained by the extra distance and multipath during the transmission path. One mitigation is to put a another reference in close vicinity to capture all those changes, therefore separate the real change in antenna property. Previous works [4, 49] used two separate tags or two tag chips with a shared antenna to do differential reading. However, we observe that the tag's sensitivity to its received power creates another layer of difficulty for reading.

Based on simulation results and preliminary testing, we find sensor code from internal auto impedance matching capacitance is reliably altered by antenna deformation yet robust to many types of interference. Thus, we focus our work on using the tag internal sensor code exclusively.

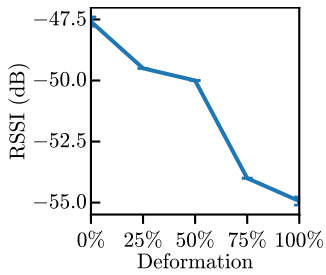

(a) Effect of deformation on RSSI. RSSI decreasess significantly with Antenna's deformation.

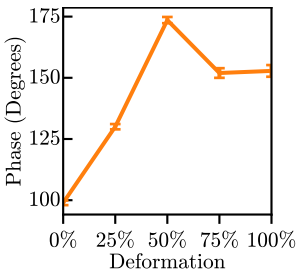

(b) Effect of deformation on phase. Phase responds to deformation in a non-monotonically way.

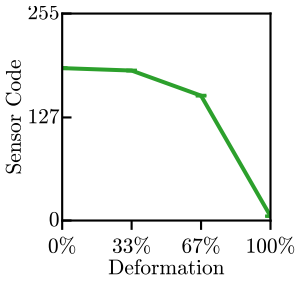

(c) Effect of deformation on sensor code. Sensor code decreases with deformation.

Figure 9: RSSI, Phase, Sensor Code Sentivity to Dipole Deformation

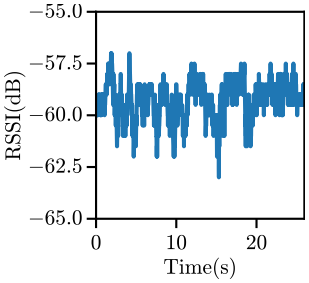

(a) Impact of dynamic environments on RSSI

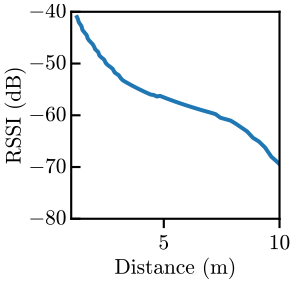

(b) Impact of distance on RSSI

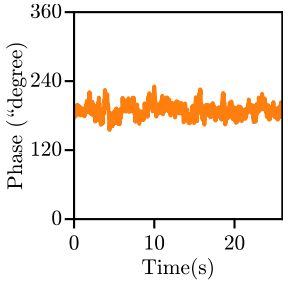

(c) Impact of dynamic environments on Phase

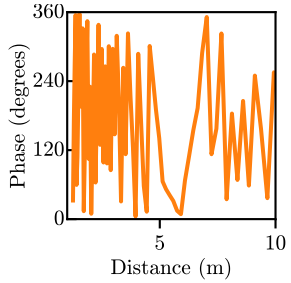

(d) Impact of distance on phase

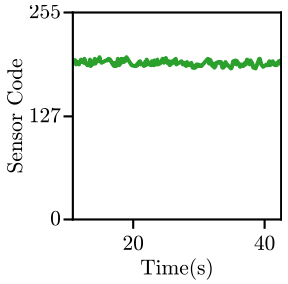

(e) Impact of dynamic environments on Sensor code

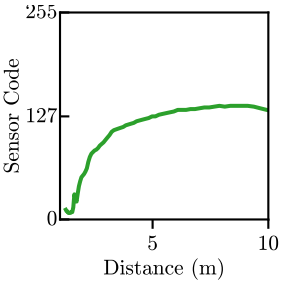

(f) Impact of distance on sensor code

Figure 10: Impact of changes in distance and moving objects nearby on different sensing features. Our results show that sensor code is much more robust than RSSI and phase.

6.2 Mitigating Effects of Excessive Receiving Power

Ideally, a sensor's reading is stable in dynamic environments and during mobility. The most influential mobility case is when the distance between reader and tag changes, as found in our feature selection experiments. It changes the radio channel drastically, especially the path loss. A lower path loss with a high reader output power will deliver too much power, causing nonlinearity and even damage.

To verify the claim that excessive receiving power can change sensing feature, we altered reader output power while fixing all other settings. The results are concluded in Figure 11a. The sensor code levels stay reliable for the lower power regime before changing violently at extremely high power. This is probably caused by internal nonlinearity of the chip. Since we require high power to achieve range and low power to read nearby tags, suitable reading power levels should be estimated and employed for different distances.

To mitigate the unwanted effects of different received power levels, we implemented a feedback loop to control the power level. It makes use of the Magnus S3's internal receiving signal strength indicator to detect the amount of power it receives. If it is beyond or below the desired range, the reader adjusts the power level to achieve the desired power level. We observe that the system is capable of reaching the desired power in a few reading cycles ($\approx$ 10 ms per cycle), and can achieve the desired receiving power level in cases with mobility.

We deployed the system and moved the tag from 4m to 1m. The distribution of resulting sensor code is concluded in Figure 11. The results with feedback control are much better than Figure 10f, where the distances varied while reader power was not dynamically adjusted. The feedback control system allows operation under different distances.

7 Evaluation

We built multiple AntSense tags with an array of configurations. They are evaluated in this section. We first evaluated the performance of the proposed system in a controlled lab environment, and then evaluated its robustness under various challenging conditions.

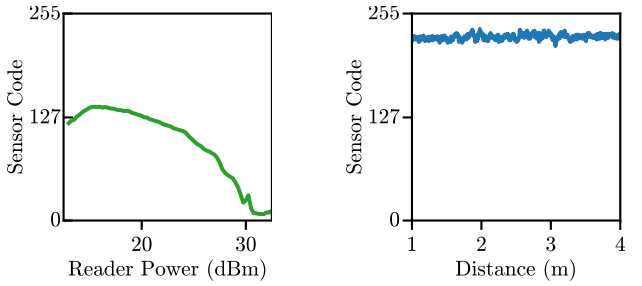

(a) Impact of reading power on sensor code with a fixed distance of 1.25 m

(b) Sensor code at different distance with feedback loop regulating power

Figure 11: Sensor code with feedback control algorithm during tag mobility. Our algorithm makes sensor code robust and stable even in short ranges.

7.1 Experiment Setup

Temperature sensors: Using shape memory alloy (SMA) material with different transition temperatures, we fabricated sensors with thresholds of 40°C, 50°C and 80°C. Other critical temperatures can be achieved with other shape memory alloy to operate in frozen and refrigerated applications.

Moisture sensors: We built multiple samples of the same moisture sensor design, with different moisture sensitivity. One moisture sensor comprises two individually built parts: a compliant mechanism and a moisture-sensitive fuse link. Compliant mechanisms were 3D-printed with FormLabs Tough 1500 resin to provide consistency. Fuse links were built with different thicknesses of the same hydro-sensitive polyvinyl alcohol (PVA) material to enable variable reaction time to moisture contact.

Weight, Size, and Cost: The complete temperature and moisture sensors weigh 1.24 and 14.5 grams, and both actuate in a 2D plane with a size of 0.5×24.5 cm^2 and 7.8×11.3 cm^2, respectively. For reference, a general-purpose RFID tag without sensing capability weighs about 1 gram with a size of less than 10×2 cm^2, while a battery-assisted temperature logging tag like CAEN A927Z can weigh 35 grams with a size of 13×2.3 cm^2. Traditional Bluetooth tag like LYWSD03MMC weighs 21 grams with a size of 4.3×4.3 cm^2. The per-unit cost of our prototype is $3.2 for temperature and $4.56 for moisture tag. Detailed break down of the cost is included in Appendix. Notably, these costs will be significantly lowered in mass production.

RFID setup: We used an off-the-shelf Impinj R420 RFID reader with an 11 dBi gain antenna filtered at 920 Mhz. The host is a laptop with an Intel Core i7-1165G7 processor. The host program controlling the reader is implemented with C# version of Impinj OctaneSDK. We only make use of this application-level programming framework with the standard EPC Gen 2 protocol. No firmware-level change is necessary, and a similar program can be easily developed for other RFID readers with respective application-level development tools. The program is responsible for decoding the read results, filtering the single tag and single operation frequency of interest, and feedback control of the reader transmit power. The PCB costs 40 cents each for our small batch prototyping, plus a negligible cost for the inductor, which will be unnecessary for printed trace based impedance matching in commercial tags.

Evaluation metrics: In each experiment, we record the time series reading of each sensor condition for at least 10 seconds. With more than 10 readings per second, this collects more than 100 data points for each sensor condition. Results presented in tables show average of these values, while results shown in line plot demonstrate means and standard deviations of them. Finally, the results shown in box plots or cumulative distribution functions (CDFs) show the distributions of the values. We evaluate our system performance in end-to-end sensing settings and various challenging environments that the system may face in real-world.

7.2 Microbenchmark

Prior to evaluating the complete system performance, we conduct several micro-benchmarks to better understand system operation characteristics. For the temperature sensor, we sweep the temperature to find out their deforming temperature. We also measure the latency between temperature exposure and sensor activation. This helps understand the dynamic performance of our sensor and the minimal duration of temperature excursion it can detect. For the moisture, we measure their response time between water contact and sensor activation. No RFID reading is in this subsection.

Threshold temperature: We measure the threshold for the temperature sensor with a few repeated heating cycles. This helps determine if the temperature sensing materials are behaving as expected and help conducting future experiments by knowing in advance correct temperature to use. We set up a heating bath with a thermostat and place the temperature sensor into that. Then we continuously heat them from room temperature (~20°C), record the temperature when deformation happens, until they all completely deform.

We report the threshold temperature in Table 1. For the thresholds of 40°C and 50°C, there temperature transitions are sharp and full deformation completed within 3°C from nominal threshold. For the 80°C one, its deformation is gradual, but full deformation is indeed achieved at its nominal temperature. Furthermore, the deformation cycle is repeated 50 times for the 50°C sensor, after which the response characteristic is consistent.

Temperature response latency: To test the response latency, we start with heating water to the threshold temperature we determined before, and then submerge our sensor into the hot water and record the video to measure the time between submersion and deformation.

The results are shown in Figure 12. We start tick at the moment the deforming region is submerged (0.0s). After half a second, the deformation is already significant (0.5s). It only takes another 2 seconds for full deformation (no more deformation from 2.0s to 2.5s). The total deformation happens within 2.5 seconds. We show the actuation latency is small enough. The actuation of the sensor itself is fast enough. For sensing air temperature change, the speed of heat transfer between tag and surrounding air will be the bottleneck. We stick to the water-bath method throughout the evaluation for its temperature consistency.

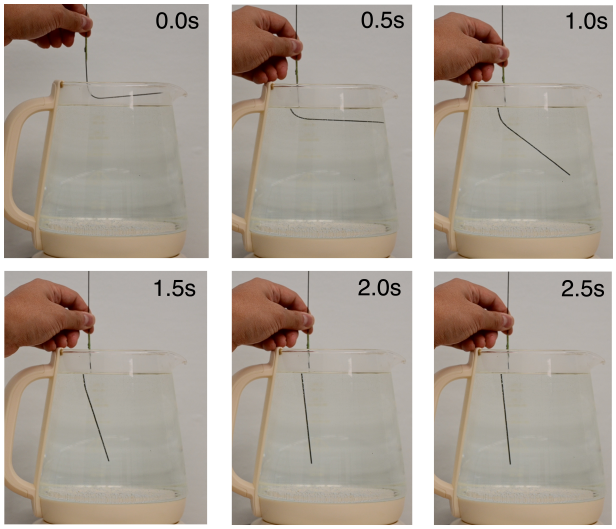

Figure 12: Responsive Time of the 50°C Temperature Tag at Water of 54°C. The tag fully deformed within 2 seconds. Because of the convex surface of the kettle, the wire appeared to be bent in the figure but actually it is fully straight.

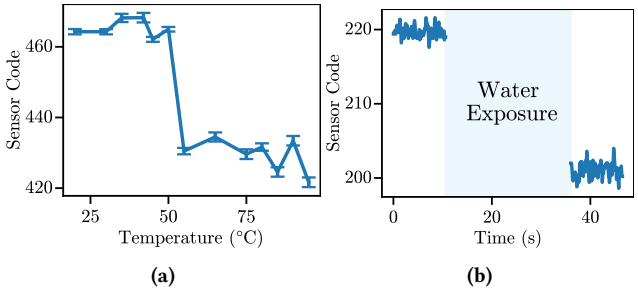

Figure 13: Sensor Code Change of a (a) Temperature and a (b) Moisture Tag. The shaded region in (b) shows the duration of exposure to the water.

Moisture response latency: Variable activation delay is desired for different applications. We build multiple pieces with the same material recipe, but with different thicknesses of hydro-sensitive link. In this way, the same sensor hardware can be dynamically repurposed for different sensitivity requirements. Using different soluble materials is another option. We measure the latency between water contact and sensor activation. In Table 2, our sensors can act extremely fast in less than 2 seconds with another one at 5 seconds, but can also achieve a slower activation of 36 seconds.

RFID read range: We measure and compare the operation range of both temperature and moisture tags pre-activation and post-activation. The temperature sensor before activation in its folded state has a read range of 4 meters. After activation, the antenna straightens and achieves a much higher read range of more than 10 meters. This agrees with our simulation results that a dipole antenna in the folded state suffers from lower gain. For the moisture sensor, as simulation predicts and experiments confirm, the read range before and after activations remains similar due to similar gain profiles. In particular, the sensor in both states can be read from 5 meters away which is sufficient for most application scenarios.

7.3 End-to-End Evaluation

We evaluate the sensors for their designated purposes, detecting temperature and moisture.

We test three temperature sensors during which they deform after crossing threshold temperature. To accurately measure the temperature and make sure that temperature of the tag has reached the threshold, we perform our measurements in a temperature controlled water bath. Before each measurement, the sensor is dried and returned to room temperature. Figure 13a demonstrates the temperature-sensing performance of the tag with thresholds of 50°C. We can clearly see a dip in sensor code output as the sensor passes threshold temperatures and activates. Both during pre-activation and post-activation, sensor readings remain stable with different temperatures. This confirms the system's ability to reliably detect temperature changes. Table 1 summarize all three temperature sensors built using the same structure with SMA of different temperature threshold. They all activated successfully at around their nominal threshold temperature and showed well measurable changes in their sensor codes.

We test the three moisture sensors by submerging them in room-temperature tap water. Figure 13b reports a sample moisture sensor recording before contacting water and after activation. The shaded blue region in the middle indicates the time period the sensor was submerged, with its width corresponding to sensor activation time. Left to the shaded region before water contact and right to the region after sensor activation, the sensor codes differ significantly, as can be seen from the step change in the average sensor code readings. The sensor has an activation delay of 36 seconds.

Table 2 summarizes results from three moisture sensors built with identical structures but different sensitivity thresholds. All sensors activated successfully near their nominal thresholds and produced measurable changes in sensor codes.

Note, since the sensors are prototyped manually, slight variations are expected, explaining the different reactions to sensor activation. Since the impedance tuning mechanism works on changing the internal parallel matching capacitance, if the change of impedance is large, or power transmission coefficient has a small derivative to capacitance, a large change is needed, while the direction of change depends on whether the nature of antenna is over-inductive or over-capacitive. Commercial manufacturing would eliminate these variations by ensuring consistent fabrication tolerances. Importantly, each sensor demonstrates significant code changes relative to its baseline, enabling reliable RFID detection.

7.4 Consistency and Robustness

We verify AntSense has robustness against various adverse environments it will face. We achieve these robustness by choosing a reliable sensing feature, sensor code, and a feedback control to dynamically find appropriate reading power. We assess this robustness in different tag orientations, tag-reader-distances, mobility in the environment, and with in different common shipping containers.

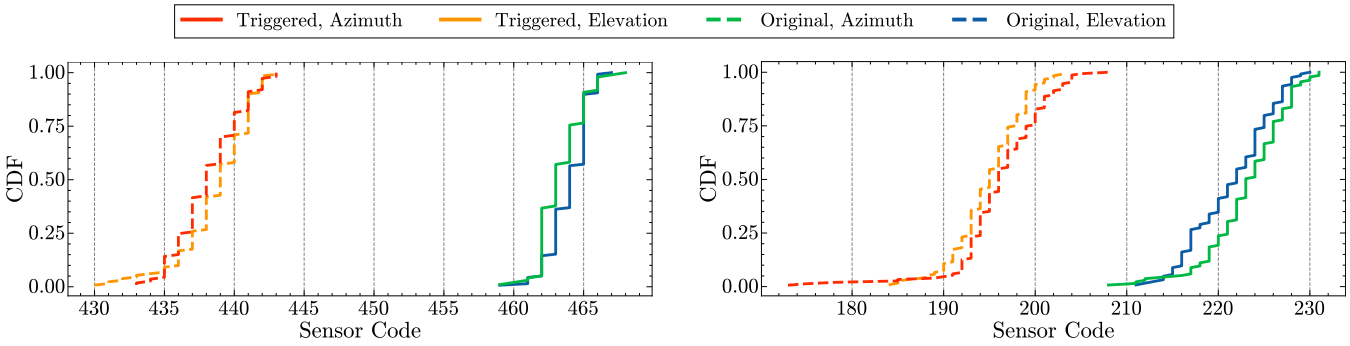

(a) Temperature Tag (b) Moisture Tag

Figure 14: Various Placement Angles. We rotate sensors from 0° to 360° in elevation and azimuth respectively, demonstrating clearly separable states. In real deployments, controlled reading angles would provide even greater separation.

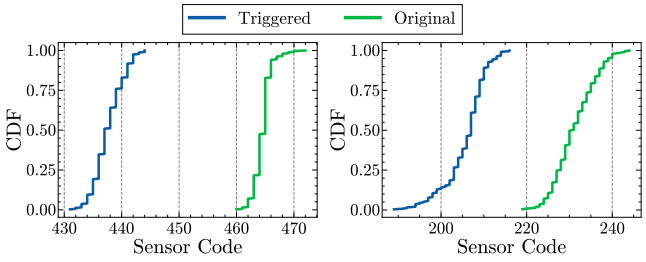

(a) Temperature Tag (b) Moisture Tag

Figure 15: Robustness with reading distances continuously swept from 1m to 5m.

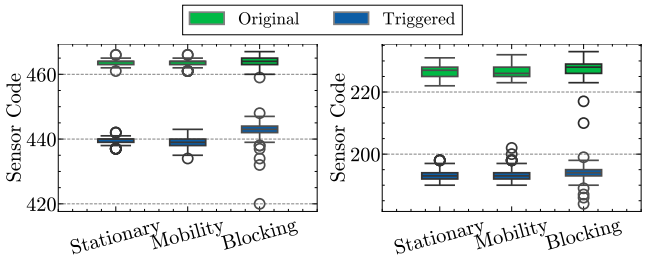

(a) Temperature Tag (b) Moisture Tag

Figure 16: Robustness in mobility environment.

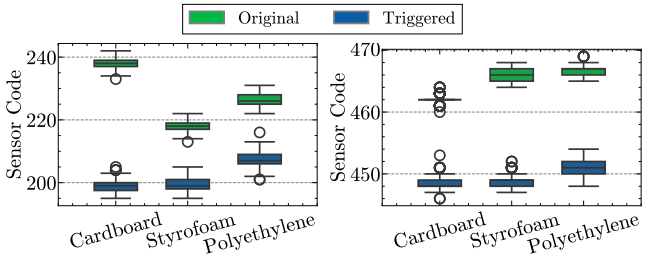

(a) Temperature Tag (b) Moisture Tag

Figure 17: Robustness in NLOS (across various shipping box materials).

Table 1: Temperature sensors with different temperature threshold

Temperature tag	#1	#2	#3
Nominal threshold	50°C	40°C	80°C
Deformation started at	50°C	40°C	72°C
Deformation completed at	53°C	42°C	79°C
Change in sensor code	35.9	21.2	23.8

Table 2: Moisture sensors with different activation time

Moisture tag	#1	#2	#3
Activation time (s)	36	5	2
Change in sensor code	18.7	243.2	64.7

Consistency with tag orientation: To make sure that the tag orientation will not cause any false positive, we rotate the tag across full 0°–360°rotations, both in azimuth and elevation, and record the sensor code reading from both original and triggered states. Figure 14 shows the cumulative distribution function (CDF) of the sensor codes across orientations. From our experiments, in both situations and both tags, the change of reading caused by change in angle does not influence the reading of state of sensors. Specifically, the separation of original and triggered state is clear, with the triggered state clustered to the left and original state clustered to the right. The separation is especially clear for the temperature tag, while slightly worse for moisture sensor. However, the two distribution is still well separated.

Consistency with tag-reader distance: We put the sensor on a cart and continuously read the sensor while moving the sensor 1m to 5m away from the antenna. Performance in Figure 15 demonstrates robustness against different distances by showing the sensor readings CDF with varied distances. As discussed before, this could be an issue if a single high reader power is used unconditionally. With our feedback loop to dynamically adjust transmit power, in effect the chip receives constant power level up until the distance

is at the maximum. Throughout the process, CDF is narrow compared to the spacing between triggered and original states. Readings will be uniform even when made at different distances, enabling massive wireless reading without needing to position sensors with precision.

Robustness in environment with mobility: Figure 16 quantifies motion resilience through stationary condition, mobility conditions (with human experimenter walking and dancing nearby) and even worse condition with blocking on the line-of-sight (the human experimenter partially blocked the antenna). The results are concluded in box plots with fliers shown. Sensors in mobile and blocking scenarios show only slightly higher distribution deviations than stationary counterparts. The small increase in reading variation does not hinder correct detection of sensor activation. The readings stay comparable across three settings. Not only the sensor itself, but also the surroundings can remain in motion during massive wireless readings while still providing accurate results.

Robustness in simulated shipping box: Finally, we evaluate the impact of different shipping box materials in which the sensor is expected to reside along with the goods. Specifically, we place the tags in cardboard, styrofoam, and polyethylene. No special care was taken in positioning the tags, simulating a realistic packing environment. These materials respectively provide collision protection, thermal insulation, and impact dampening in a shipping context. The results are presented in Figure 17. In every condition, the change due to sensor triggering is still clearly separated. But different material does cause reading shifts and the numbers are no longer comparable across materials. This is because antenna is sensitive to the electric and magnetic field distribution around it, both in gain and impedance. During shipping, sensors are expected to reside in the original shipping container all the way until unpacking, so the sensor will perform reliably.

These experiments validate the system's operational robustness. In the anticipated use case of long-distance shipping, the sender scan all tags once and record EPCs and sensing codes, without paying unnecessary attention to orientation, reading distance or keeping the environment stationary. At arrival, the recipient scan all received packages without opening them, match the EPCs with original sensing codes, and immediately be aware of any spoiled packages.

8 Related Works

We explore the other works in enabling persistent remote sensing, including traditional sensors and RFID-based sensors.

8.1 Traditional Sensors

Many sensors are commercially available to sense various environmental parameters such as temperature and moisture. Temperature sensors include thermocouples, resistance temperature detectors (RTDs), or thermistors. Depending on the application, different materials are used in their fabrication, such as fiber-based sensors [9, 29, 35] in high-temperature scenarios, composite materials in wearable devices [50, 55]. Moisture sensors detect moisture through various methods, such as capacitance changes [2, 23] and resistance changes [48]. They are connected to active circuits for readings and communication.

Despite their widespread usage and applications , these sensors have two major drawbacks. First, they require active circuits for reading and communication, preventing them from operating without a battery. Second, they lack persistence; as a result, retaining their measurements necessitates additional memory components, which increase both cost and power consumption. In contrast, AntSense enables persistent, batteryless sensing.

8.2 RFID Sensors

UHF RFID tags are widely used in logistics, and their potential applications in sensing have been actively explored using different approaches such as connecting a traditional sensor to an RFID tag or using the tag itself as a sensor.

RFID tag equipped with a Sensor. Past work has proposed to use RFID as a communication mechanism for sensors. In this approach, sensing and communication functions are separated, with the RFID harvesting energy and enabling communication while external sensors and a microcontroller handle measurements. For example, The WISP [33] can attach various external sensors. However, these RFIDs are more expensive and require close proximity to an RFID reader to harvest enough energy, a limitation that persists even in optimized commercial tags [28]. Moreover, these approaches cannot enable persistent sensing without having any batteries, which significantly increases their cost and scalability.

There are also commercial battery-powered RFID sensors like Axzon AZN5200, CAEN RT0005, and CAEN A927Z which can record and store temperature data digitally. The historical data is then accessible via RFID. Although this approach offers persistent sensor measurements at high accuracy, the battery requirement significantly increases their initial and maintenance cost and creates negative environmental impacts.

RFID tag as a sensor: Past work has also shown that the RFID tag itself can serve as a sensor, with a reader interpreting the sensory outputs using phase, RSS, or sensor code [6, 12, 43, 49, 52]. They are used for measuring soil moisture [49], environmental conditions [12, 43], object displacement [6], respiration [52] and food&liquid quality [15]. However, they all are memoryless and do not enable persistent batteryless sensing. There are works explore persistent batteryless sensing. Nevertheless, some require custom readers for chipless RFID [18, 31]. Some require multiple readings from multiple tags [5, 7, 13], which suffer from varying radio environments and can have degraded robustness. Therefore, none of them can be deployed into a commercially feasible product.

RFID with stimuli-responsive material: Finally, some past work has also used stimuli-response material or antenna deformation as a modality to sense environment parameters such as structure health monitoring [16], gas concentration [44], and crack detection [30]. However, they cannot be read with standard RFID protocols. Some require measuring wideband RF parameters (such as the resonance frequency of the antenna), which is not possible with commercial RFID readers or require changing RFID protocol, making it non-compliant with FCC. The closest work to AntSense is the system proposed by Caizzone et al. [7] where they use two RFID chips with one being shorted by glued SMA initially. The activation of the SMA breaks the short circuit and allows both

chips to be read. However, this solution has three major limitations. First, the breakage of the bonding glue makes the sensor not easily reusable. Second, their reading is inherently binary (i.e., the tag is responding or not) which limits its capability and reliability. Finally, since other factors such as signal blockage can also cause the chip not responding, they can have high false positive readings. A more general issue with multi-chip approaches is that they cannot be read fast and reliably in environments with many RFID tags. This is due to the fact that RFID reading suffers from collision when a large number of tags are present. Moreover, since the RFID protocol performs frequency hopping while RSSI and phase are only comparable when they are read at the same frequency and channel, we need wait until both tags are read successfully in the same round and same channel. Hence, these systems have a huge latency in reading the sensor unless the RFID protocol is modified such that it does not do frequency hopping, which will not be comply with FCC.

In contrast, AntSense is compatible with commercial RFID readers and systems while providing trustworthy readings against signal blockage for binary classification of moisture and temperature change events.

9 Discussion

In this section, we discuss some practical aspects of our system. We also discuss limitations of our design and propose potential solutions to enhance its applicability in real-world scenarios.

Tag reusability: One advantage of AntSense's tag is reusability characteristic. In particular, our tags can be reset after triggering with minimal manual effort and be reused for subsequent shipments. For example, the temperature sensor can be restored by re-bending the shape-memory alloy into its original U-shape, while the moisture sensor's bonding element can be easily replaced using low-cost, mass-produced components. This modularity also enables per-shipment tuning of moisture sensitivity by selecting inserts with different break forces.

Tag deployment: AntSense's tag may suffer from unintended actuation caused by external mechanical factors. To avoid this from happening, the tags can be placed in a protective container. This would protect the tag from external mechanical sources while the tag can still operate normally as the temperature or moisture changes.

Sustainability: AntSense is fully compliant with the UHF RFID reader ecosystem as we only extend the tag design. Therefore, no reader-side infrastructure change is needed. Furthermore, our tag design is also compatible with other widely available self-tuning UHF RFID ICs that provide on-chip sensing readouts (e.g., the Impinj Monza R6 [51], Impinj M730/750/830/850 series [20], and NXP UCODE 8/9 series [40]). This supply diversity lowers risk and simplifies procurement.

Dual-modality sensing on a single tag: Our current design uses two separate tags for temperature and moisture. A desirable extension is a single tag that hosts two stimuli-responsive elements (e.g., temperature and moisture) to enable dual-modality sensing. To achieve this, one can carefully co-design mechanical elements and RF matching circuit such that the tag realizes four separable mechanical states: {*none*, *A-only*, *B-only*, *both*}. This enables the tag to respond with four different ranges in sensor code, where they represent the change in temperature and moisture.

Finer Sensing Granularity: We currently evaluate the ability of AntSense in binary detection of single violation events. However, the 9-bit measurement ability of the chip and our design have a potential to enable fine granularity in both moisture and temperature sensing. We were unable to test this since our prototypes were manually manufactured and soldered. The lack of consistency makes it hard to characterize the sensor collectively. However, even with inconsistency, a difference of 20 units in sensor code provides sufficient robustness for reliable event detection across different environments. On the other hand, commercial fabrication would significantly improve fabrication consistency. Mass-produced tags can use printed matching networks and direct chip connections to offer much tighter manufacturing tolerances. This enhanced consistency would enable full utilization of the 0-to-511 measurement range, supporting fine-grained sensing capabilities such as recording exact maximum temperature value or moisture percentage .

10 Conclusion

This paper introduces AntSense, a novel passive RFID sensor system that leverages stimuli-responsive materials to persistently record environmental threshold violations without batteries or continuous reader presence. By integrating shape memory alloys and water-soluble polymers with RFID chip capable of impedance detection, AntSense enables wireless detection of past temperature and moisture excursions even after conditions have normalized. AntSense bridges a critical gap in supply chain monitoring by providing a scalable, maintenance-free solution for verifying product integrity throughout transit. Finally, although this paper focuses on threshold violation detection (i.e. binary classification), the 9-bit reading capability of the underlying hardware can be further extended to temperature and moisture measurements with finer sensing granularity and other value of interest.

APPENDIX: AntSense's Tags Cost Analysis

The cost of AntSense tags consists of three parts: Magnus-S3 chip, mounting board, and stimuli-sensitive actuator. Chips and mounting circuits are shared between temperature and moisture versions. The chip costs $2 each (retail price) for prototyping, and can be as low as $0.54 per unit when purchased in bulk. Mounting boards are currently regular rigid PCBs that host the chip and match the antenna, costing $0.40 each. For the stimuli-sensitive structures, the temperature sensor uses SMA costing $1 per foot of material from Amazon retail. Our design uses 0.8 feet per sensor, bringing the material cost to $0.80 per tag. The moisture sensor uses 14.50 grams of 3D printing resin priced at $149/kg retail, or $2.16 each. This cost can be reduced with cheaper 3D printing materials (e.g., ABS at ~$20/kg, $0.30 each) or with injection molding. In total, the per-unit cost of our experimental prototypes is $3.2 for temperature and $4.56 for moisture, which can be significantly lowered in mass production.

References

[1] Martim L. Aguiar, Pedro D. Gaspar, Pedro D. Silva, Luísa C. Domingues, and David M. Silva. 2022. Real-Time Temperature and Humidity Measurements

during the Short-Range Distribution of Perishable Food Products as a Tool for Supply-Chain Energy Improvements. *Processes* 10, 11 (Nov. 2022), 2286.

[2] Norah Alsadun, Sandeep Surya, Kamlesh Patle, Vinay S. Palaparthy, Osama Shekhah, Khaled N. Salama, and Mohamed Eddaoudi. 2023. Institution of Metal–Organic Frameworks as a Highly Sensitive and Selective Layer In-Field Integrated Soil-Moisture Capacitive Sensor. *ACS Applied Materials & Interfaces* 15, 4 (Feb. 2023), 6202–6208.

[3] Axzon. 2025. *Packaged ICs*. Axzon. https://www.axzon.com/packagedQFN.html Accessed: 1 July 2025.

[4] Nagarjun Bhat, Agrim Gupta, Ishan Bansal, Harine Govindarajan, and Dinesh Bharadia. 2024. ZenseTag: An RFID assisted Twin-Tag Single Antenna COTS Sensor Interface. In *Proceedings of the 22nd ACM Conference on Embedded Networked Sensor Systems* (Hangzhou, China) *(SenSys '24)*. Association for Computing Machinery, New York, NY, USA, 336–350.

[5] Rahul Bhattacharyya, Claudio Di Leo, Christian Floerkemeier, Sanjay Sarma, and Lallit Anand. 2010. RFID tag antenna based temperature sensing using shape memory polymer actuation. In *SENSORS, 2010 IEEE*. 2363–2368. https://doi.org/10.1109/ICSENS.2010.5690951

[6] R. Bhattacharyya, C. Floerkemeier, and S. Sarma. 2009. Towards tag antenna based sensing - An RFID displacement sensor. In *2009 IEEE International Conference on RFID*. IEEE, Orlando, FL, 95–102.

[7] Stefano Caizzone, Cecilia Occhiuzzi, and Gaetano Marrocco. 2011. Multi-Chip RFID Antenna Integrating Shape-Memory Alloys for Detection of Thermal Thresholds. *IEEE Transactions on Antennas and Propagation* 59, 7 (July 2011), 2488–2494. https://doi.org/10.1109/TAP.2011.2152341

[8] Sejin Choi, Youngho Eom, Seon-Mi Kim, Da-Woon Jeong, Jongmin Han, Jun Mo Koo, Sung Yeon Hwang, Jeyoung Park, and Dongyeop X. Oh. 2020. A Self-Healing Nanofiber-Based Self-Responsive Time-Temperature Indicator for Securing a Cold-Supply Chain. *Advanced Materials* 32, 11 (2020), 1907064.

[9] Chen-Shane Chu and Yu-Lung Lo. 2008. A Plastic Optical Fiber Sensor for the Dual Sensing of Temperature and Oxygen. *IEEE Photonics Technology Letters* 20, 1 (Jan. 2008), 63–65.

[10] Ahmet Yunus Cil, Dini Abdurahman, and Ibrahim Cil. 2022. Internet of Things Enabled Real Time Cold Chain Monitoring in a Container Port. *Journal of Shipping and Trade* 7, 1 (May 2022), 9.

[11] Andrea De Silvestri, Enrico Ferrari, Simone Gozzi, Francesca Marchi, and Roberto Foschino. 2018. Determination of Temperature Dependent Growth Parameters in Psychrotrophic Pathogen Bacteria and Tentative Use of Mean Kinetic Temperature for the Microbiological Control of Food. *Frontiers in Microbiology* 9 (Dec. 2018), 3023.

[12] Debi Dutta, Simone Genovesi, Giuliano Manara, and FIlippo Costa. 2024. Characterization of Material Properties by Using an Auto-Tuned RFID Chip. In *Proceedings of the 4th URSI Atlantic RadioScience Conference – AT-RASC 2024*. URSI – International Union of Radio Science, Gran Canaria, Spain.

[13] Jinlan Gao, Johan Sidén, Hans-Erik Nilsson, and Mikael Gulliksson. 2013. Printed humidity sensor with memory functionality for passive RFID tags. *IEEE Sensors Journal* 13, 5 (2013), 1824–1834.

[14] Jiaming Guo, Xinyu Wei, Bin Li, Yongfeng Cao, Jiawei Han, Xinting Yang, and Enli Lü. 2020. Characteristic Analysis of Humidity Control in a Fresh-Keeping Container Using CFD Model. *Computers and Electronics in Agriculture* 179 (Dec. 2020), 105816.

[15] Unsoo Ha, Junshan Leng, Alaa Khaddaj, and Fadel Adib. 2020. Food and liquid sensing in practical environments using {RFIDs}. In *17th USENIX symposium on networked systems design and implementation (NSDI 20)*. 1083–1100.

[16] Yuan He, Meng Meng Li, Guo Chun Wan, and Mei Song Tong. 2020. A Passive and Wireless Sensor Based on RFID Antenna for Detecting Mechanical Deformation. *IEEE Open Journal of Antennas and Propagation* 1 (2020), 426–434. https://doi.org/10.1109/OJAP.2020.3015782

[17] I-Hsuan Hong, Jr-Fong Dang, Yi-Hsuan Tsai, Chen-Shen Liu, Wang-Tsang Lee, Ming-Li Wang, and Pei-Chun Chen. 2011. An RFID application in the food supply chain: A case study of convenience stores in Taiwan. *Journal of Food Engineering* 106, 2 (2011), 119–126.

[18] Sheikh Dobir Hossain, Miguel A. Palacios Mora, Annatoma Arif, Bhushan Lohani, and Robert C. Roberts. 2022. Flexible Chipless RFID Temperature Memory Sensor. In *2022 IEEE International Conference on Flexible and Printable Sensors and Systems (FLEPS)*. 1–4. https://doi.org/10.1109/FLEPS53764.2022.9781599

[19] Impinj, Inc. 2025. *Impinj Speedway RAIN RFID eRaders for the Internet of Things*. https://www.impinj.com/products/readers/impinj-speedway Accessed: 1 July 2025.

[20] Impinj, Inc. 2025. *RAIN RFID Tag Chips for the Internet of Things*. https://www.impinj.com/products/tag-chips Accessed: 1 July 2025.

[21] Shaojun Jiang, Sumei Jia, and Hongjun Guo. 2024. Internet of Things (IoT)-Enabled Framework for a Sustainable Vaccine Cold Chain Management System. *Heliyon* 10, 7 (April 2024), e28910.

[22] Umit Kartoglu and Henry Ames. 2022. Ensuring Quality and Integrity of Vaccines throughout the Cold Chain: The Role of Temperature Monitoring. *Expert Review of Vaccines* 21, 6 (June 2022), 799–810.

[23] Shenawar Ali Khan, Muhammad Saqib, Maryam Khan, Muhammad Muqeet Rehman, Sheik Abdur Rahman, and Woo Young Kim. 2023. Wide-Range, Fast-Responsive Humidity Sensor Based on In_2Se_3 /PEDOT:PSS Nanocomposite. *ACS Applied Electronic Materials* 5, 8 (Aug. 2023), 4473–4484.

[24] Sameer Kumar, Eric Swanson, and Thuy Tran. 2009. RFID in the healthcare supply chain: usage and application. *International journal of health care quality assurance* 22, 1 (2009), 67–81.

[25] Nitesh K. Kunda, Denis Wafula, Meilinn Tram, Terry H. Wu, and Pavan Muttil. 2016. A Stable Live Bacterial Vaccine. *European Journal of Pharmaceutics and Biopharmaceutics* 103 (June 2016), 109–117.

[26] Likitha Lasantha, Nemai C. Karmakar, and Biplob Ray. 2023. Chipless RFID Sensors for IoT Sensing and Potential Applications in Underground Mining—A Review. *IEEE Sensors Journal* 23, 9 (2023), 9033–9048.

[27] Bin Li, Jiaming Guo, Jingjing Xia, Xinyu Wei, Hao Shen, Yongfeng Cao, Huazhong Lu, and Enli Lü. 2020. Temperature Distribution in Insulated Temperature-Controlled Container by Numerical Simulation. *Energies* 13, 18 (Jan. 2020), 4765.

[28] Songfan Li, Qianhe Meng, Yanxu Bai, Chong Zhang, Yihang Song, Shengyu Li, and Li Lu. 2023. Go Beyond RFID: Rethinking the Design of RFID Sensor Tags for Versatile Applications. In *Proceedings of the 29th Annual International Conference on Mobile Computing and Networking*. ACM, Madrid Spain, 1–16.

[29] C. R. Liao and D. N. Wang. 2013. Review of femtosecond laser fabricated fiber Bragg gratings for high temperature sensing. *Photonic Sensors* 3, 2 (June 2013), 97–101.

[30] Adi Mahmud Jaya Marindra and Gui Yun Tian. 2018. Chipless RFID Sensor Tag for Metal Crack Detection and Characterization. *IEEE Transactions on Microwave Theory and Techniques* 66, 5 (2018), 2452–2462. https://doi.org/10.1109/TMTT.2017.2786696

[31] Marcos Martinez and Daniel van der Weide. 2017. Chipless RFID temperature threshold sensor and detection method. In *2017 IEEE International Conference on RFID (RFID)*. 61–66. https://doi.org/10.1109/RFID.2017.7945588

[32] Rohan Menon, Rohit Gujarathi, Ali Saffari, and Joshua R Smith. 2022. Wireless identification and sensing platform version 6.0. In *Proceedings of the 20th ACM Conference on Embedded Networked Sensor Systems*. 899–905.

[33] Rohan Menon, Rohit Gujarathi, Ali Saffari, and Joshua R. Smith. 2022. Wireless Identification and Sensing Platform Version 6.0. In *Proceedings of the 20th ACM Conference on Embedded Networked Sensor Systems*. ACM, Boston Massachusetts, 899–905.

[34] Maad M Mijwil, Kamal Kant Hiran, Ruchi Doshi, and Omega John Unogwu. 2023. Advancing Construction with IoT and RFID Technology in Civil Engineering: A Technology Review. *Al-Salam Journal for Engineering and Technology* 2, 2 (2023), 54–62.

[35] Md. Aslam Mollah, S.M. Riazul Islam, Md. Yousufali, Lway Faisal Abdulrazak, Mb. Biplob Hossain, and I.S. Amiri. 2020. Plasmonic temperature sensor using D-shaped photonic crystal fiber. *Results in Physics* 16 (March 2020), 102966.

[36] Liu Han Ng, Jordy Kim Ung Ling, and Kunn Hadinoto. 2022. Formulation Strategies to Improve the Stability and Handling of Oral Solid Dosage Forms of Highly Hygroscopic Pharmaceuticals and Nutraceuticals. *Pharmaceutics* 14, 10 (Sept. 2022), 2015.

[37] Fred Niederman, Richard G. Mathieu, Roger Morley, and Ik-Whan Kwon. 2007. Examining RFID applications in supply chain management. *Commun. ACM* 50, 7 (July 2007), 92–101.

[38] P.V. Nikitin and K.V.S. Rao. [n. d.]. Theory and measurement of backscattering from RFID tags. 48, 6 ([n. d.]), 212–218.

[39] Haifeng Niu and S. Jagannathan. 2013. High memory passive RFID tags with multimodal sensor design and application to asset monitoring in-transit. In *2013 IEEE International Instrumentation and Measurement Technology Conference (I2MTC)*. 1615–1619. https://doi.org/10.1109/I2MTC.2013.6555687

[40] NXP Semiconductors. 2025. *UCODE® RAIN RFID*. NXP Semiconductors. https://www.nxp.com/products/rfid-nfc/ucode-rain-rfid-uhf Accessed: 1 July 2025.

[41] C. Paggi, C. Occhiuzzi, and G. Marrocco. 2014. Sub-Millimeter Displacement Sensing by Passive UHF RFID Antennas. *IEEE Transactions on Antennas and Propagation* 62, 2 (2014), 905–912.

[42] Amitangshu Pal and Krishna Kant. 2020. Smart Sensing, Communication, and Control in Perishable Food Supply Chain. *ACM Transactions on Sensor Networks* 16, 1 (Feb. 2020), 1–41.

[43] Francesco Piccinno, Federica Naccarata, Riccardo Colella, Francesco P. Chietera, Luca Catarinucci, and Gaetano Marrocco. 2023. Exploiting Self-Tunable RFID Chips for Wireless Sensing of Permittivity to Enable Passive Low-Cost Food-Quality Monitoring Systems. In *2023 IEEE 13th International Conference on RFID Technology and Applications (RFID-TA)*. IEEE, Aveiro, Portugal, 45–48.

[44] Radislav A Potyrailo and Cheryl Surman. 2013. A passive radio-frequency identification (RFID) gas sensor with self-correction against fluctuations of ambient temperature. *Sensors and Actuators B: Chemical* 185 (2013), 587–593.

[45] Swadhin Pradhan, Eugene Chai, Karthikeyan Sundaresan, Lili Qiu, Mohammad A Khojastepour, and Sampath Rangarajan. 2017. Rio: A pervasive rfid-based touch gesture interface. In *Proceedings of the 23rd Annual International Conference on Mobile Computing and Networking*. 261–274.

[46] Abdi Pratama Putra, Muhammad Yusro, and Aodah Diamah. 2022. Prototype of a Monitoring System for Temperature, Humidity, and Location of Reefer Container Based on IoT. In *2022 International Conference on Informatics Electrical and Electronics (ICIEE)*. 1–5.

[47] Jussi Rahola. 2008. Power Waves and Conjugate Matching. *IEEE Transactions on Circuits and Systems II: Express Briefs* 55, 1 (Jan. 2008), 92–96.

[48] Lingli Shen, Wanqi Feng, Dan Yu, and Wei Wang. 2024. Hydrophobically Coated Fabric Moisture Sensor with the Gas/Liquid Water Detection Function. *ACS Applied Polymer Materials* 6, 17 (Sept. 2024), 10357–10367.

[49] Ju Wang, Liqiong Chang, Shourya Aggarwal, Omid Abari, and Srinivasan Keshav. 2020. Soil moisture sensing with commodity RFID systems. In *Proceedings of the 18th International Conference on Mobile Systems, Applications, and Services*. ACM, Toronto Ontario Canada, 273–285.

[50] Jiahui Wang, Yanjing Sun, Pan Jia, Jingxuan Su, Xin Zhang, Na Wu, Haitao Yu, Yanlin Song, and Jinming Zhou. 2023. Wearable nanocomposite hydrogel temperature sensor based on thermally-switchable and mechanical-deformation-insensitive structural colors. *Chemical Engineering Journal* 476 (Nov. 2023), 146602.

[51] Konstantinos Zannas, Hatem El Matbouly, Yvan Duroc, and Smail Tedjini. 2018. Self-tuning RFID tag: A new approach for temperature sensing. *IEEE Transactions on Microwave Theory and Techniques* 66, 12 (2018), 5885–5893.

[52] Jintao Zhang, Jiexiao Yu, Yongtao Ma, and Xiuyan Liang. 2021. RF-RES: Respiration Monitoring With COTS RFID Tags by Dopplershift. *IEEE Sensors Journal* 21, 21 (Nov. 2021), 24844–24854.

[53] Haochen Zhao, Mohammad Iman Mokhlespour Esfahani, Suresh Krishnan, and Omid Abari. 2024. A Passive Back Posture Monitoring System Using Orthogonal RFID Design. *IEEE Sensors Journal* 24, 21 (2024), 35610–35620.

[54] Ningli Zhu, Yuhua Xia, Ying Liu, Chuanzhen Zang, Hai Deng, and Zhenzhou Ma. 2018. Temperature and Humidity Monitoring System for Bulk Grain Container Based on LoRa Wireless Technology. In *Cloud Computing and Security*, Xingming Sun, Zhaoqing Pan, and Elisa Bertino (Eds.). Springer International Publishing, Cham, 102–110.

[55] Zhengfang Zhu, Yi Su, Jing Chen, Jinyong Zhang, Lixin Liang, Zedong Nie, Wei Tang, Yongsheng Liang, and Hui Li. 2024. PEDOT:PSS-Based Wearable Flexible Temperature Sensor and Integrated Sensing Matrix for Human Body Monitoring. *ACS Applied Materials & Interfaces* (Oct. 2024), acsami.4c11251.

[56] Zhixin Zong, Salil D. Desai, Aditya M. Kaushal, Dewey H. Barich, Hong-Shian Huang, Eric J. Munson, Raj Suryanarayanan, and Lee E. Kirsch. 2011. The Stabilizing Effect of Moisture on the Solid-State Degradation of Gabapentin. *AAPS PharmSciTech* 12, 3 (July 2011), 924.